JOURNAL OF GEOPHYSICAL RESEARCH, VOL. 113, A07221, doi:10.1029/2008JA013267, 2008

Magnetic coupling of the ring current and the radiation belt

Y. Ebihara,[1] M.-C. Fok,[2] J. B. Blake,[3] and J. F. Fennell[3]

Received 7 April 2008; revised 16 June 2008; accepted 18 June 2008; published 30 July 2008.

[1] The magnetic influence of the storm time ring current on high-energy particles is demonstrated by using a simulation of the ring current incorporating self-consistent magnetic and electric fields. Observations by the Polar satellite show that the magnetic field is occasionally depressed by 50% or more near the equatorial plane at <6 R_E. We call them equatorially magnetic depression events (EMDEs) and focus on the most intense EMDE observed during an intense storm on 22 October 1999. The simulation predicts that under a strong convection electric field, the magnetic field strength is highly depressed around $L = 5$ by newly injected ions of energy 80 keV or less. The depressed magnetic field causes a significant adiabatic decrease in the high-energy ion flux at pitch angles near 90° to conserve the first adiabatic invariant. A more tail-like (shortened) magnetic field line causes an enhancement of the flux at pitch angles near 0° and 180° to conserve the second adiabatic invariant. Consequently, a butterfly-like pitch angle distribution (PAD) is formed, which agrees with the Polar observation. We propose that the adiabatic process could have acted not only on the high-energy component of the protons but also on relativistic electrons in the outer radiation belt. This notion is supported by simultaneous Polar observation of relativistic electron fluxes that show a decrease at pitch angles near 90° and a slight increase at pitch angles near 0° and 180°. PADs of protons and electrons can be used to distinguish nonadiabatic processes acting selectively on electrons from adiabatic ones.

Citation: Ebihara, Y., M.-C. Fok, J. B. Blake, and J. F. Fennell (2008), Magnetic coupling of the ring current and the radiation belt, *J. Geophys. Res.*, *113*, A07221, doi:10.1029/2008JA013267.

1. Introduction

[2] Fluxes of the energetic particles in the outer radiation belt sometimes show a variation that is correlated with the *Dst* index. Since the *Dst* index is widely used as a proxy of a measure of the ring current, the *Dst*-correlated variation of the flux is called the "ring current effect" [*McIlwain*, 1966]. The ring current effect appears not only in energetic electron fluxes [e.g., *Dessler and Karplus*, 1961; *McIlwain*, 1966; *Williams et al.*, 1968; *Li et al.*, 1997; *Nakamura et al.*, 1998; *Shprits et al.*, 2006] but also in energetic ion fluxes [e.g., *Lyons and Williams*, 1976; *Williams*, 1981b; *Fu et al.*, 2001].

[3] For ions, the ring current effect appears typically at energies of ~100 keV and above. On the basis of observations by Explorer 45, *Lyons and Williams* [1976] showed that the ion flux at energies less than 63 keV increased while the ion flux at energies greater than 382 keV decreased at a radial distance of 4 R_E near the equatorial plane during an intense storm. *Lyons* [1977] showed butterfly like pitch angle distributions (PADs) of >200 keV protons and >50 keV electrons simultaneously observed by Explorer 45 near $L = 4$ near the equatorial plane during the intense magnetic storm of 17 December 1971. The evolution of the PADs is quantitatively explained as a result of conservation of the first two adiabatic invariants. *Williams* [1981b] observed the same tendency in the data from ISEE 1, namely an increase in ion energy density at low energy (24–210 keV) and a decrease at high energy (>210 keV). *Williams* [1981a] suggested that high-energy ions respond adiabatically to magnetic field changes caused by low-energy ion enhancements. That is, low-energy ions (constituting the storm time ring current) and high-energy particles (including the radiation belt particles) can be tightly coupled through the local magnetic field.

[4] Many efforts have been made to explain the adiabatic changes quantitatively using empirical models of the ring current-induced magnetic field [e.g., *Söraas and Davis*, 1968; *Lyons and Williams*, 1976; *Kim and Chan*, 1997; *Nakamura et al.*, 1998]. Most of the calculations have used empirical magnetic field models that are a function of the geocentric distance and *Dst*. However, it is not so simple to investigate the magnetic coupling of the ring current and energetic particle fluxes because of the following four reasons. First, the storm time ring current depends entirely on time and magnetic local time (MLT) [e.g., *Brandt et al.*, 2002; *Le et al.*, 2004]. Second, the ions that constitute the

[1] Institute for Advanced Research, Nagoya University, Nagoya, Japan.
[2] NASA Goddard Space Flight Center, Greenbelt, Maryland, USA.
[3] Space Sciences Department, Aerospace Corporation, Los Angeles, California, USA.

0148-0227/08/2008JA013267$09.00

Table 1. Equatorially Magnetic Depression Events Observed by the Polar Satellite in 1996–2001

		Position			Magnetic Field					
Date	UT[a]	R (Re)	MLAT (deg)	MLT (h)	Observed (nT)	IGRF Model (nT)	Magnetic Depression Rate[b]	Dst (nT)	Storm Phase[c]	Pitch Angle (100 keV proton)
7 Nov 1998	1315	5.3	4.2	22.4	96	215	−0.55	−56	EMP	butterfly
9 Nov 1998	1828	4.8	1.4	22.1	124	279	−0.55	−142	LMP	butterfly
22 Sep 1999	1953	5.7	−3.3	1.0	76	164	−0.54	18	IP	butterfly
22 Oct 1999	0017	5.0	2.7	22.9	75	226	−0.67	−23	EMP	butterfly
11 Nov 1999	0633	5.4	3.9	21.9	89	195	−0.54	−55	LMP	butterfly
11 Jan 2000	1837	5.5	4.2	17.1	69	177	−0.61	−34	EMP	butterfly
23 Jan 2000	0026	5.2	2.0	16.1	88	210	−0.58	−97	LMP	almost isotropic
14 Jul 2000	1739	5.6	−14.2	5.1	82	199	−0.59	−2	NST	butterfly

[a]UT at which the most intense magnetic depression rate was recorded.
[b]Magnetic depression rate is given by $(|\mathbf{B}_{OBS}|-|\mathbf{B}_{IGRF}|)/|\mathbf{B}_{IGRF}|$, where $\mathbf{B}_{OBS}$ is the observed magnetic field and $\mathbf{B}_{IGRF}$ is the magnetic field modeled by IGRF.
[c]Storm phases of IP, EMP, LMP, and NST denote, initial phase, early main phase, late main phase, and nonstorm time, respectively.

ring current also undergo adiabatic acceleration/deceleration [e.g., *Lyons and Williams*, 1976]. Third, the ring current-induced magnetic field alters the grad-B and curvature drift velocities of all the trapped particles [e.g., *Ebihara and Ejiri*, 2000]. Fourth, equatorial magnetic fields can be depressed [e.g., *Akasofu et al.*, 1961; *Hoffman and Bracken*, 1965; 1967] and distance between mirror points can be shortened by the ring current. When the magnetic field becomes tail-like, the field line length between the ionosphere and the equatorial plane will be shorter. In addition, when the equatorial magnetic field is depressed, mirror point altitudes in both hemispheres will be higher at a given equatorial pitch angle to conserve the first adiabatic invariant. Both magnetic changes will result in adiabatic acceleration in the field-aligned direction to conserve the second adiabatic invariant. In order to fully investigate the ring current effect, it is necessary to model the three-dimensional magnetic field that is balanced with the plasma pressure (the ring current).

[5] Several ring current simulations incorporating a self-consistent magnetic field have been developed. *Lemon et al.* [2004] obtained a force-balanced magnetic field by solving a set of ideal magnetohydrodynamic (MHD) equations with a frictional dissipation term. *Chen et al.* [2006] traced equatorially mirroring ions under a self-consistent magnetic field with an equatorial PAD which is assumed to be sinusoidal. They found that the ring current energization is suppressed by the ring current-induced magnetic field. *Zaharia et al.* [2006] solved quasi-2-D elliptic equations to obtain a self-consistent magnetic field expressed by the Euler potential. They found large depressions of the plasma pressure on the nightside compared with that obtained using a dipole magnetic field.

[6] This paper presents recently obtained simulation results on the magnetic coupling of low-energy ions (which are regarded as the storm time ring current) and high-energy ions (which are regarded as a proxy of the radiation belt) as a first step toward developing a sophisticated and realistic model of the radiation belt. In particular, we focus on the PAD of particles as a quantitative measure of the ring current effect. We extended the kinetic ring current simulation (called the comprehensive ring current model [*Fok et al.*, 2001]) that solves the evolution of the phase space density of ions and the electric potential to incorporate a force-balanced magnetic field in a self-consistent manner. Simulation results are compared with the PAD measured by the Polar satellite near the equatorial plane.

2. Observation

[7] The Polar satellite was launched in 1996 into a highly elliptical polar orbit with apogee of about 9 R_E, perigee of about 1.8 R_E, and orbital period of about 18 h. The apogee was initially over the northern polar region, but it has moved toward the equator at about 16° per year. The Magnetospheric Ion Composition Sensor (MICS) [*Wilken et al.*, 1992; *Roeder et al.*, 2005], which is one of the components of the Charge and Mass Magnetospheric Ion Composition Experiment (CAMMICE) on the Polar satellite, uses an electrostatic analyzer together with a solid-state detector to measure the energy, time of flight, and energy per charge of ion fluxes in the energy range between 6 keV/q and 200 keV/q. The Comprehensive Energetic Particle and Pitch Angle Distribution (CEPPAD) experiment [*Blake et al.*, 1995] provides proton and electron angular distributions in the energy range between ∼20 keV and ∼10 MeV.

[8] To investigate the magnetic coupling of the ring current and the energetic particles, we selected magnetic depression events in the Polar data during which the following four criteria are satisfied. (1) The magnetic depression rate defined by $(|\mathbf{B}_{OBS}| - |\mathbf{B}_{IGRF}|)/|\mathbf{B}_{IGRF}|$ is less than −0.5, where $\mathbf{B}_{OBS}$ is the magnetic field observed by the Magnetic Field Experiment (MFE) [*Russell et al.*, 1995] on the Polar satellite and $\mathbf{B}_{IGRF}$ is the magnetic field modeled by the International Geomagnetic Reference Field (IGRF). (2) The radial distance of the Polar satellite is less than 6 R_E. (3) The Polar satellite is in the magnetosphere. (4) Data from MICS is available. In total, eight events were identified between 1996 and 2001, which are summarized in Table 1. Hereafter, we refer to them as equatorially magnetic depression events (EMDEs) because they were found near the equatorial plane. In most cases, EMDEs are found to occur during magnetic storms and are accompanied by a butterfly-like PAD for a 100 keV proton flux. In this paper, we focus on the most intense EMDE that was observed around 0017 UT on 22 October 1999.

[9] Figure 1 shows the magnetic field and proton fluxes observed by Polar as it crossed the equatorial plane during a magnetically quiet period just before the intense EMDE of 22 October 1999. The *Dst* index ranged between 15 and

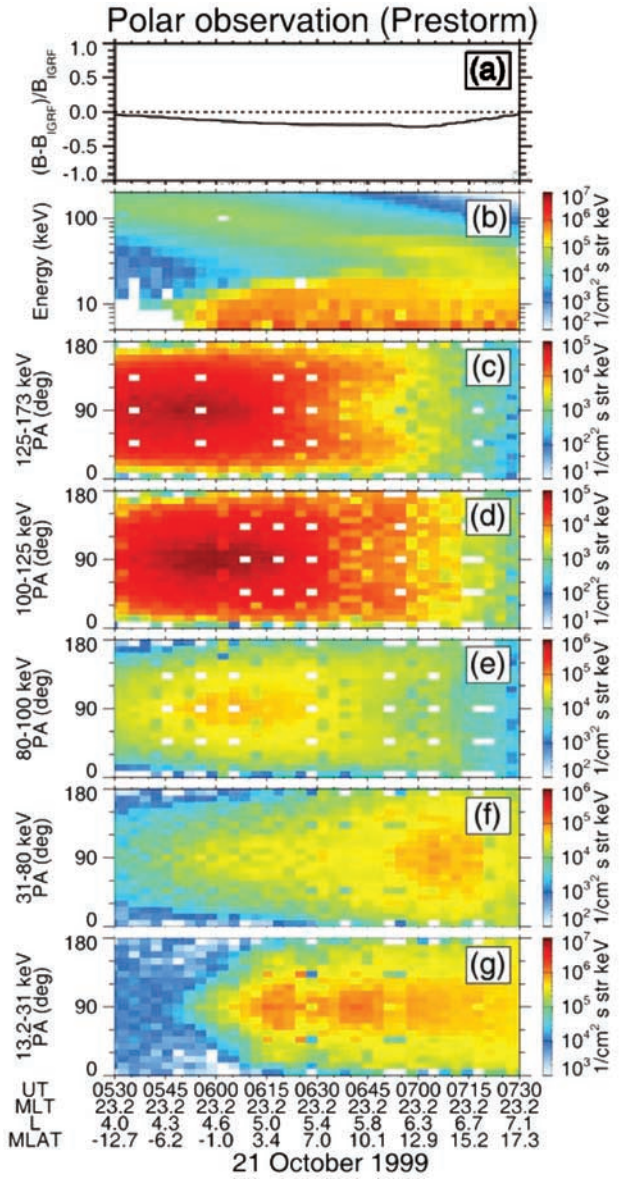

Figure 1. Polar observation during the equatorial plane crossing just before the equatorially magnetic depression event (EMDE) of 22 October 1999. (a) Depression ratio $(|\mathbf{B}_{OBS}| - |\mathbf{B}_{IGRF}|)/|\mathbf{B}_{IGRF}|$, (b) spin-averaged differential flux of protons, pitch angle distribution of proton flux at (c) 125–173 keV, (d) 100–125 keV, (e) 80–100 keV, (f) 31–80 keV, and (g) 13.2–31 keV. The orbital information, MLT in hours, L value in R_E, and MLAT in degrees are indicated at the bottom of the figure.

17 nT, and the Z component of the interplanetary magnetic field (IMF) ranged between 11 and 21 nT during this period. The Polar satellite was in the outbound path, moving from the Southern Hemisphere to the Northern Hemisphere near the geomagnetic meridian of 23.2 MLT. Figure 1a shows the magnetic depression ratio $(|\mathbf{B}_{OBS}| - |\mathbf{B}_{IGRF}|)/|\mathbf{B}_{IGRF}|$, indicating that the magnetic field is less depressed within less than 21%. The depression of the magnetic field is probably due to a weak ring current and a weak tail current.

[10] In Figure 1b, the spin-averaged differential flux of protons measured by Polar/MICS is displayed. Protons appear to consist of two distinct energy components; the high- (low-) energy component that appears in the energy range above (below) a few tens of keV. The major characteristic of the energy versus L spectrogram of the protons is consistent with that statistically obtained one [e.g., *Orsini et al.*, 1994]. The characteristic energy of the high-energy component is ~100 keV at $L = 4.3$, which is decreasing with L-value. The low-energy component appears at $L > 4.5$. The inner edge of the low-energy component exhibits a nose-like energy dispersion [*Smith and Hoffman*, 1974], which is a consequence of competition between the magnetic drift and the $E \times B$ drift under the large-scale convection electric field [*Ejiri et al.*, 1980]. The nose-like

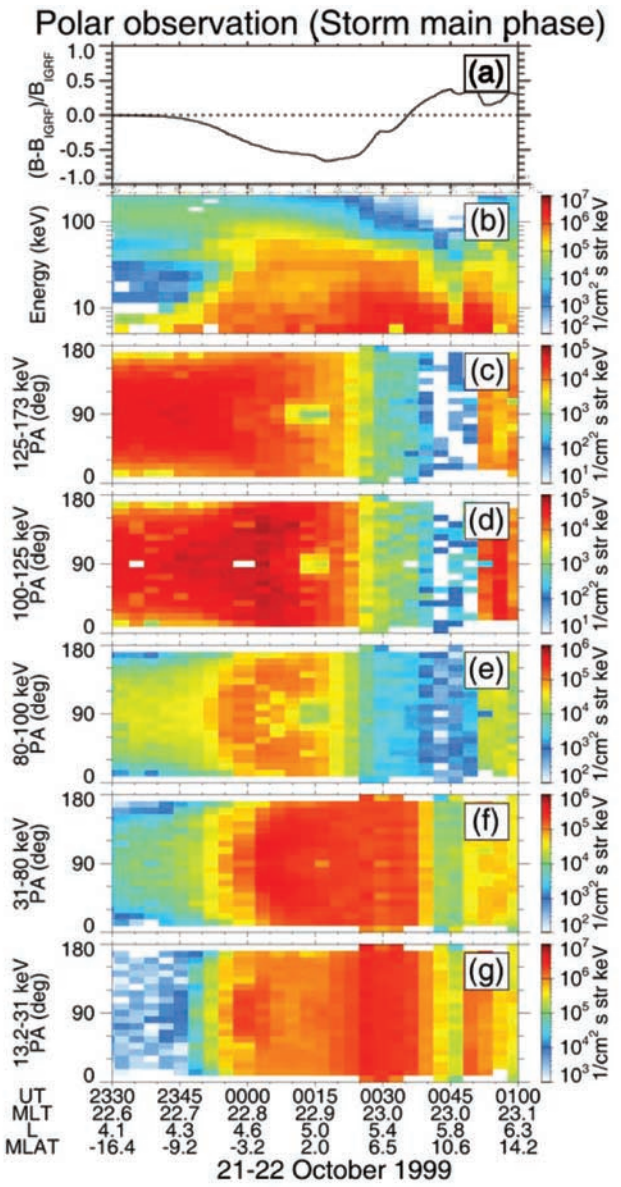

Figure 2. Same as Figure 1 except for the most intense EMDE that occurred in the subsequent orbit. The observation was made during the storm main phase of 22 October 1999.

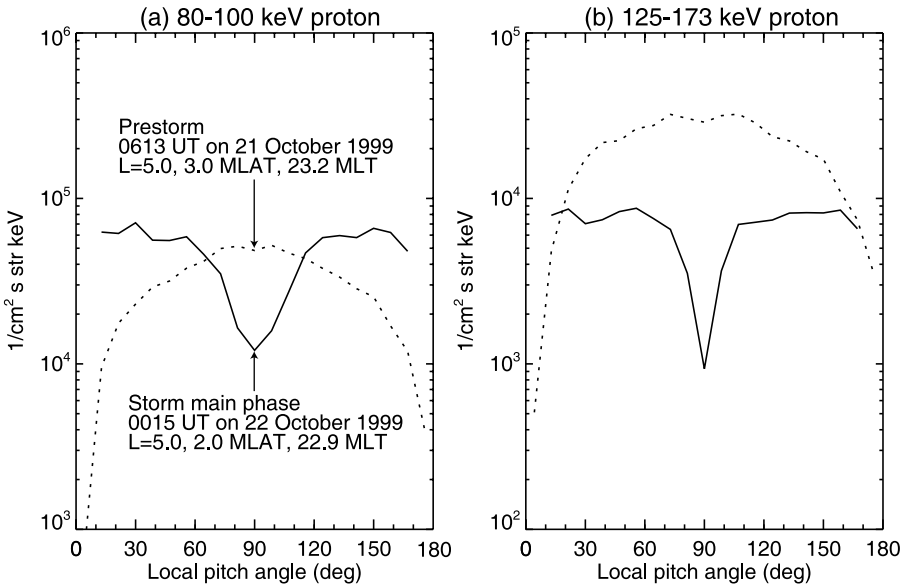

Figure 3. Pitch angle distribution of protons measured by Polar/MICS for (a) 80–100 keV and (b) 125–173 keV. Solid and dotted lines indicate the differential flux at 0613 UT on 21 October 1999 (prestorm condition) and 0015 UT on 22 October 1999 (storm main phase), respectively.

dispersion could also be interpreted as the time-of-flight effects of the drifts of different energy protons [*Li et al.*, 2000]. PADs versus time spectrograms of the protons are shown in the last five panels of Figure 1. The PAD is almost pancake-like with maximum at 90° or isotropic at all energies except for that with 125–173 keV at L = 5.8–6.5 in which the magnetic field is slightly depressed probably due to a weak tail current.

[11] Figure 2 summarizes the magnetic field and proton fluxes observed by Polar during the subsequent crossing of the equatorial plane on 21–22 October 1999. The *Dst* index started decreasing around 0000 UT on 22 October 1999 in accordance with the southward turning of the interplanetary magnetic field (IMF) around 2325 UT and reached a minimum (−237 nT) around 0600 UT on 22 October 1999. Thus, the interval shown in Figure 2 covers the early main phase of the intense storm. Figure 2a indicates that the magnetic field is highly depressed by 62% at L = 5.0 near the equatorial plane. In Figure 2b, the low-energy component of the spin-averaged proton flux is shown to significantly increase at $L > 4.3$ in comparison with the preceding pass as shown in Figure 1b. The enhancement of the proton flux occurs in the energy range up to ∼80 keV, which is thought to be responsible for the storm time ring current [e.g., *Krimigis et al.*, 1985].

[12] PAD versus time spectrograms of the protons are shown in the last five panels of Figure 2. The PAD is almost pancake-like at all energies until 2345 UT. However, the situation drastically changes around 0010 UT. The proton flux at energies greater than 80 keV shows an abrupt drop near the local pitch angle of 90° at $L \sim 5$ (at 0015 UT) as shown in Figures 2c–2e. The 31–80 keV proton flux also shows a slight drop near the local pitch angle of 90° (Figure 2f). The transition between the pancake-like PAD and the butterfly-like PAD takes place independent of kinetic energy.

[13] Figure 3 compares the proton PADs observed in the prestorm condition (0613 UT on 21 October 1999) and the storm main phase (0015 UT on 22 October 1999). They were observed by Polar/MICS at L = 5.0 and 23.2 MLT near the equatorial plane. The proton fluxes at 80–100 keV and 125–173 keV are displayed on the left and right, respectively. The PAD is pancake-like in the prestorm condition, while it becomes butterfly-like in the storm main phase. The flux at a pitch angle of 90° decreases to ∼25% at 80–100 keV and ∼3% at 125–173 keV in comparison with the prestorm condition. The flux of protons at pitch angles around 13° is shown to increase significantly.

[14] The same tendency is seen in the energetic electrons simultaneously observed by Polar/CEPPAD. Figure 4 compares the PADs of electrons at 1698–2101 keV in the prestorm condition (0613 UT on 21 October 1999) and the storm main phase (0015 UT on 22 October 1999). The electron flux at a pitch angle of 90° is shown to decrease by about 2 orders of magnitude in comparison between the prestorm and main phase conditions. The flux at pitch angles around 10° is shown to increase slightly.

3. Simulation

[15] We have extended the comprehensive ring current model (CRCM) [*Fok et al.*, 2001] to incorporate a self-consistent magnetic field in the inner magnetosphere. Hereafter, we refer to this simulation as the extended CRCM (ECRCM). The original CRCM solves the temporal and spatial evolution of the phase space density of ions using the bounce-averaged approximation under a Tsyganenko-type empirical magnetic field model [*Tsyganenko*, 1995; *Tsyganenko and Stern*, 1996]. The electric field in the inner magnetosphere is calculated by solving Poisson's equation for given height-integrated conductivities and field-aligned currents driven by the plasma pressure (ring current). We

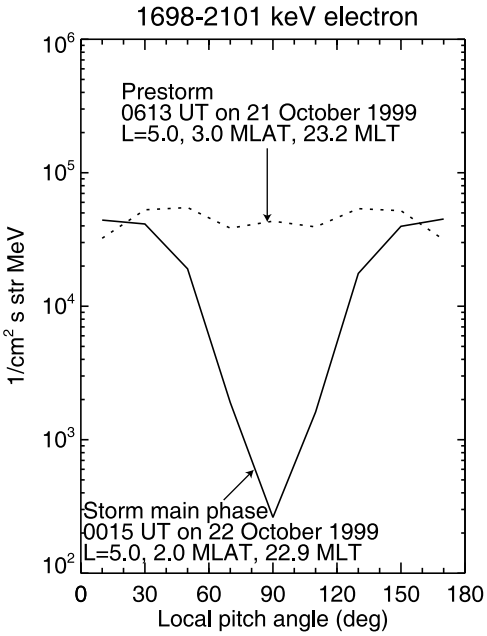

Figure 4. Pitch angle distribution of electrons measured by Polar/CEPPAD for 1698–2101 keV. Solid and dotted lines indicate the differential flux at 0613 UT on 21 October 1999 (prestorm condition) and 0015 UT on 22 October 1999 (storm main phase), respectively.

assumed that the ring current could change the electric field significantly at $L \leq 6.5$ due to the ring current-driven field-aligned current. In the dipole field, the L value of 6.5 is mapped to the magnetic latitude of 66.7 MLAT at the ionospheric altitude that is assumed to be 100 km. The electric potential at the poleward boundary at 66.7 MLAT was determined by the Weimer 2001 empirical convection model [*Weimer*, 2001], depending on the solar wind velocity, density, and IMF. The background conductivity was calculated using an empirical ionospheric model of the International Reference Ionosphere (IRI-95) [*Bilitza*, 1997] and an empirical thermospheric model of the mass spectrometer incoherent scatter (MSIS-E90) models [*Hedin*, 1991]. The aurora-associated conductivity was given by an empirical model dependant on *Kp* [*Hardy et al.*, 1987]. In ECRCM, following the method introduced by *Akasofu et al.* [1961] and *Hoffman and Bracken* [1965], the magnetic field induced by the ring current is calculated using the Biot–Savart law. For the purpose of simulating the localized deformation of the magnetic field near the equatorial plane, we implicitly assume that the localized deformation in the inner magnetosphere is primarily caused by the ring current and there is little contribution from the current flowing at and beyond the simulation outer boundary.

[16] The electric current perpendicular to the magnetic field (which is the general expression of the ring current) is given by the equation

$$\mathbf{J}_\perp = \frac{\mathbf{B}}{B^2} \times \left[\nabla P_\perp + (P_\parallel - P_\perp) \frac{(\mathbf{B} \cdot \nabla)\mathbf{B}}{B^2} \right], \qquad (1)$$

where $\mathbf{B}$ is the magnetic field at $\mathbf{r}$ and $P_\perp$ and $P_\parallel$ are the perpendicular plasma pressure and the parallel plasma pressure, respectively. The magnetic field induced by the ring current is calculated using the Biot–Savart law as

$$\mathbf{B}_{\mathrm{RC}}(\mathbf{r}) = \frac{\mu_0}{4\pi} \int\int\int \frac{\mathbf{J}_\perp(\mathbf{r}') \times (\mathbf{r} - \mathbf{r}')}{|\mathbf{r} - \mathbf{r}'|^3} d^3 r'. \qquad (2)$$

After calculating $\mathbf{B}_{\mathrm{RC}}$, we updated the magnetic field by summing the three components of the magnetic field as $\mathbf{B} = \mathbf{B}_{\mathrm{DIPOLE}} + \mathbf{B}_{\mathrm{TSY1996}} + \mathbf{B}_{\mathrm{RC}}$, where $\mathbf{B}_{\mathrm{DIPOLE}}$ is the dipole magnetic field and $\mathbf{B}_{\mathrm{TSY1996}}$ is the external magnetic field given by the Tsyganenko 1996 model [*Tsyganenko*, 1995; *Tsyganenko and Stern*, 1996]. The updated $\mathbf{B}$ is substituted into (1). Following the calculations of *Hoffman and Bracken* [1967] and *Berko et al.* [1975], we repeated this procedure three times. *Berko et al.* [1975] showed that the magnetic field calculated with three iterations approached the observed magnetic field. We confirmed that three iterations are sufficient because calculations with four or five iterations reach almost the same result as the three-iteration calculation.

[17] At the beginning of the simulation, the magnetosphere was filled with particles having a distribution function based on the AMPTE/CCE measurements for a quiet time [*Sheldon and Hamilton*, 1993] with isotropic PAD. For this particular run, we held the boundary condition of the protons constant to be an isotropic Maxwellian distribution with a density of 0.3 cm^{-3} and a temperature of 3 keV at $L = 10$. The solar wind and IMF data obtained using the 5-min resolution of OMNI provided by NASA/GSFC/NSSDC was used to drive the Weimer 2001 model. In order to illuminate the effect of $\mathbf{B}_{\mathrm{RC}}$, the external magnetic field $\mathbf{B}_{\mathrm{TSY1996}}$ [*Tsyganenko*, 1995; *Tsyganenko and Stern*, 1996] was held constant to be the condition at 0000 UT on 22 October 1999, that is, the solar wind dynamic pressure of 5.33 nPa, *Dst* of −23 nT, IMF *By* of −6.7, and IMF *Bz* of −10 nT. In the simulation, the phase space density of the protons, the electric potential, and the magnetic field were updated every 10 s.

4. Results

[18] Figure 5 summarizes the simulation results for the magnetic field, plasma pressure $P_\perp$, and perpendicular current density $J_\perp$ at 2345 UT on 21 October 1999 (Figures 5a–5e) and at 0015 UT on 22 October 1999 (Figures 5f–5j). The pressure and current density are drawn in the meridian plane of 2300 MLT. At 2345 UT, the plasma pressure had just started to be enhanced due to the strongly enhanced convection electric field (Figure 5d). At 0015 UT, the Polar satellite was near the equatorial plane and could have encountered the region filled with the enhanced plasma pressure (Figure 5i) and the perpendicular current density (Figure 5j). The field lines passing through at 4–6 R_E in the equatorial plane are shown to be more tail-like, and their roots at the ionosphere altitude are slightly displaced toward the equator (Figures 5i and 5j). In addition, the equatorial magnetic field is highly depressed at a radial distance of ~3.5–5.0 R_E (Figure 5g). A depressed magnetic field near the equatorial plane raises a mirror point altitude, which results in a shortened distance between mirror points in the both hemispheres. These magnetic field changes should

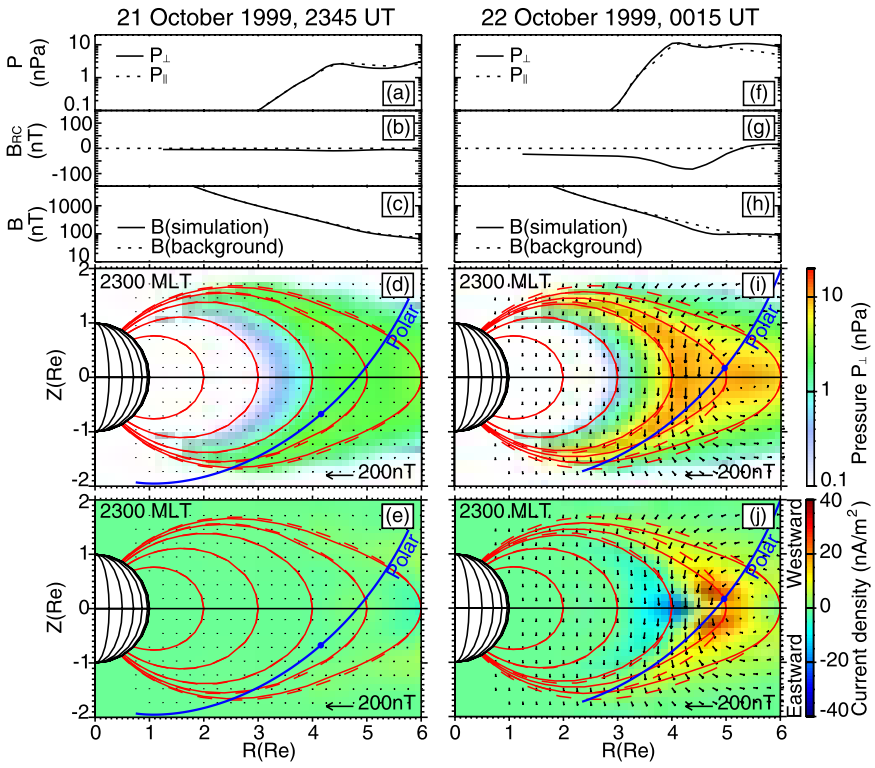

Figure 5. From top to bottom are shown (a, f) equatorial plasma pressure $P_\perp$ and $P_\parallel$, (b, g) equatorial magnetic field induced by the simulated ring current B_{RC}, (c, h) equatorial total magnetic field B, (d, i) perpendicular plasma pressure $P_\perp$ at the magnetic meridian plane of 2300 MLT, and (e, j) perpendicular current density $J_\perp$ (positive westward) at the magnetic meridian plane of 2300 MLT, displayed for (left) 2345 UT on 21 October 1999 and (right) 0015 UT on 22 October 1999. The blue curve represents the Polar orbit projected onto the meridian plane of 2300 MLT and the filled blue dot shows the Polar position. The solid red lines and dashed red lines indicate simulated and background magnetic field lines, respectively. B(simulation) and B(background) denote the magnetic fields given by $|\mathbf{B}_{DIPOLE} + \mathbf{B}_{T1996} + \mathbf{B}_{SIM}|$ and $|\mathbf{B}_{DIPOLE} + \mathbf{B}_{T1996}|$, respectively. An arrow indicated in Figures 5d, 5e, 5i, and 5j represents a $\mathbf{B}_{SIM}$ vector.

influence charged particles when the first two adiabatic invariants are conserved.

[19] Figure 6 summarizes the magnetic field and proton fluxes along the virtual Polar orbit in the simulation box. To make a direct comparison with the observation, Figure 6 includes both spatial and temporal variations, and the format is the same as that of Figure 2. The only exception is that the virtual Polar satellite flew in the equatorial plane. The MLT and L value are the same as those of the real Polar orbit, but MLAT is held constant at zero. The reason why the virtual satellite flew in the equatorial plane is to illuminate the effect of the magnetic field changes on the equatorial PADs and to avoid the effect of different magnetic latitudes. Since our major focus is on the butterfly like PAD observed near the equatorial plane around 0015 UT, having the virtual satellite fly on the equatorial plane has no significant impact on conclusions.

[20] Figure 6a represents the magnetic depression ratio given by $(|\mathbf{B}_{SIM}| - |\mathbf{B}_{DIPOLE}|)/|\mathbf{B}_{DIPOLE}|$, where $\mathbf{B}_{SIM}$ is the simulated magnetic field. The minimum magnetic depression ratio is about -0.62, which is close to the observed ratio of -0.67. To separate spatial and temporal variations of it, the magnetic depression ratio at four selected times is presented in Figure 7. At 2330 UT (a solid line), the ratio reaches minimum value of -0.53 at $L = 5.3$, which is primarily determined by the Tsyganenko 1996 model. At 0015 UT (a dash-dotted line), the ratio reaches minimum value of -0.66 at $L = 4.8$.

[21] Figure 6b displays an energy versus time spectrogram of the pitch angle-averaged flux of protons. Proton fluxes at energies less than ~80 keV are well enhanced, which is consistent with the observation. For example, the inner edge of the newly enhanced protons at 10 keV is located around $L = 4.2$ at 2340 UT. The perpendicular plasma pressure in the equatorial plane at $L = 5$ also increases from 2 nPa at 2345 UT on 21 October 1999 to 10 nPa at 0015 UT on 22 October 1999.

[22] PAD versus time spectrograms of the simulated protons are shown in the last five panels of Figure 6. At high energies (90–149 keV), the PADs are pancake-like before 2345 UT, whereas they become butterfly-like at 0010 UT. As for low energies (22–55 keV), the PADs remain to be almost isotropic or pancake-like. The transition energy between the pancake-like and butterfly-like PADs

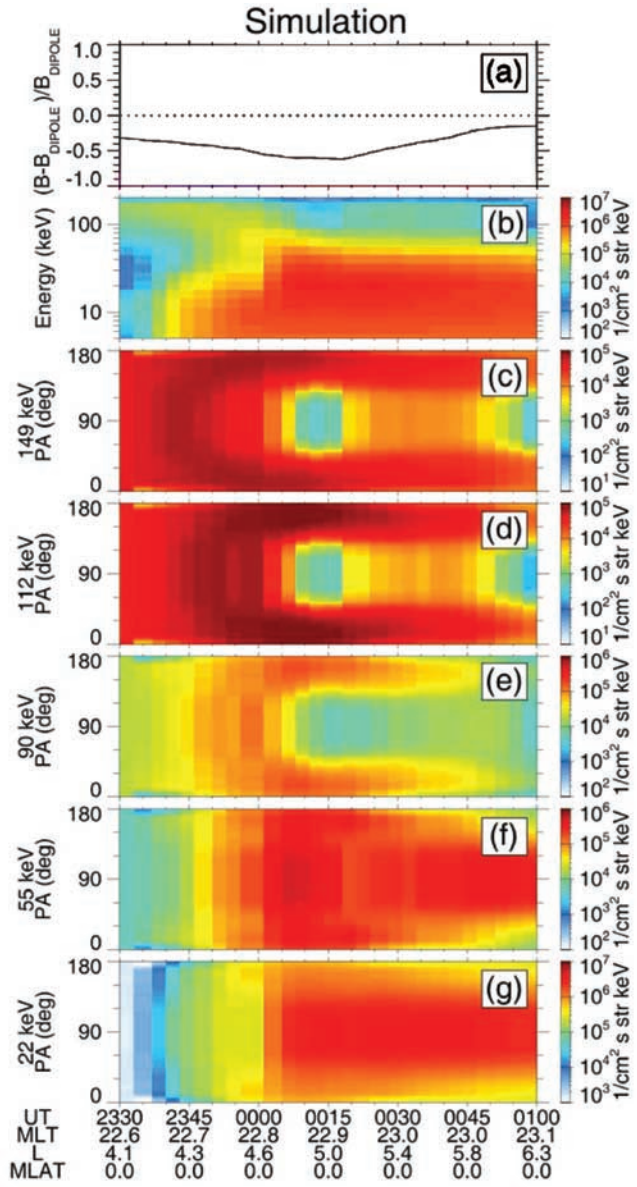

Figure 6. Same as Figure 2 except that obtained along the Polar orbit in the simulated ring current in the equatorial plane. The top panel shows the magnetic depression ratio given by $(|\mathbf{B}_{SIM}| - |\mathbf{B}_{DIPOLE}|)/|\mathbf{B}_{DIPOLE}|$.

occurs between 55 and 90 keV, which is consistent with the observation.

[23] Figure 8 shows the temporal variation of the simulated PADs of 80–100 keV and 125–173 keV protons at $L = 5$ and 22.9 MLT in the equatorial plane at four selected times. At 2330 UT, the PAD is almost isotropic because the simulation started with the isotropic PAD as an initial condition. As time proceeds, the proton flux at pitch angles near 90° decreases, while that at pitch angles near 0° and 180° increases. Finally, the PAD becomes butterfly-like. This tendency is consistent with observation as shown in Figure 3. In the simulation, the flux at pitch angles near 90° decreases due to adiabatic deceleration of the equatorially mirroring protons to conserve the first adiabatic invariant under the depressed magnetic field. The flux at pitch angles near 0° and 180° increases due to adiabatic acceleration of the field-aligned protons to conserve the second adiabatic invariant under the tail-like (and shortened) magnetic field lines.

5. Discussion

[24] Since the adiabatic change is independent of mass and charge, it is speculated that high-energy electrons should also undergo an adiabatic change and show a butterfly-like PAD, although we did not solve the electron flux simultaneously with that of the protons in the simulation. This notion is supported by the Polar/CEPPAD observations shown in Figure 4. The PADs of energetic electrons had a near isotropic shape just before the magnetic storm, whereas they became butterfly-like when the low-energy proton fluxes (<80 keV) were enhanced.

[25] Satellites have observed butterfly-like PADs for high-energy protons and electrons on the nightside [e.g., *Pfitzer et al.*, 1969; *West et al.*, 1973; *Baker et al.*, 1978; 1981a; 1981b; *Lyons*, 1977; *Sibeck et al.*, 1987; *Selesnick and Blake*, 2002; *Fritz et al.*, 2003]. Some of them have been attributed to magnetopause shadowing due to the drift trajectories depending on the pitch angle under an asymmetric magnetic field (drift shell splitting) [e.g., *Stone*, 1963; *Roederer*, 1967]. The magnetopause shadowing can explain the abrupt decrease in the particle fluxes at pitch angles near 90°, whereas it hardly explains the increase in the flux at pitch angles near 0° and 180°. It seems to be reasonable to consider the butterfly-like PADs shown in

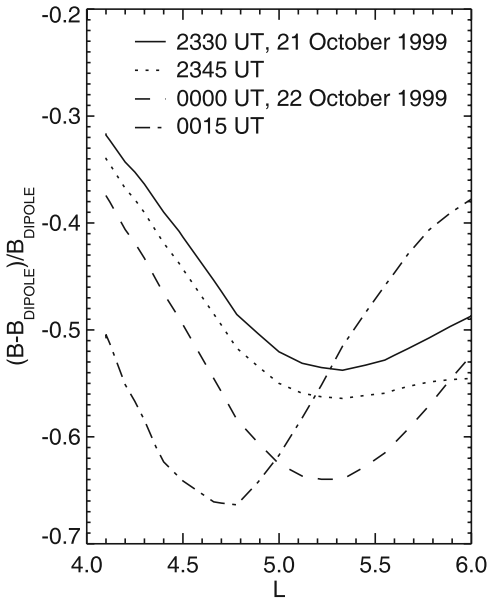

Figure 7. Temporal evolution of the magnetic depression ratio given by $(|\mathbf{B}_{SIM}| - |\mathbf{B}_{DIPOLE}|)/|\mathbf{B}_{DIPOLE}|$ along the Polar orbit in the simulated ring current in the equatorial plane at 2330 UT on 21 October 1999, 2345 UT, 0000 UT on 22 October 1999 and 0015 UT.

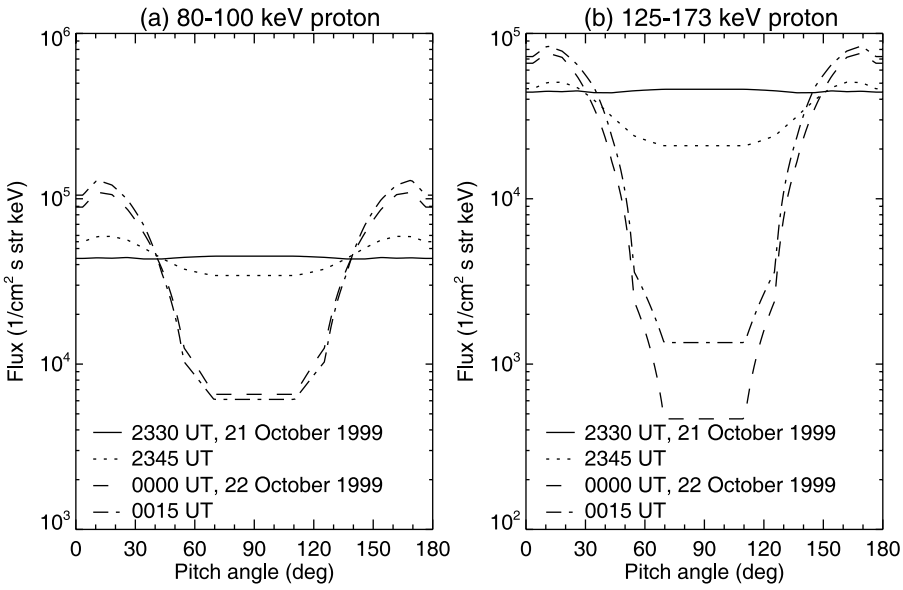

Figure 8. Temporal evolution of the simulated PAD of proton fluxes with energy at (a) 80–100 keV and (b) 125–173 keV at L = 5 and 22.9 MLT in the equatorial plane. Solid, dotted, dashed, and dash-dotted lines indicate the differential flux at 2330 UT on 21 October 1999, 2345 UT, 0000 UT on 22 October 1999 and 0015 UT, respectively.

Figures 3 and 4 as a consequence of the adiabatic change of energetic particles because the flux at pitch angles near 0° and 180° increases when the flux at pitch angles near 90° decreases. Of course, we cannot deny other possibilities such as magnetopause shadowing.

[26] In the inner radiation belt ($L \sim 2$), the Akebono satellite observed a dumbbell-like distribution of relativistic electrons (>1 MeV) near the equatorial plane [*Morioka et al.*, 2001]. They concluded that the dumbbell-like distribution resulted from intense quasi-electrostatic UHR mode waves that were simultaneously observed by the Akebono satellite. The ring current is most likely difficult to result in the dumbbell-like distribution observed in the inner radiation belt where the magnetic energy is much stronger than the particle energy.

[27] It is noted that the depression of the simulated proton fluxes at 80–100 keV and 125–173 keV at pitch angles near 90° (Figure 8) are much greater in magnitude and wider in pitch angle than the observed depressions (Figure 3). The most likely reason for the disagreement between simulation and observation is that a pitch angle scattering process, which is not considered in our simulation, occurs in the real magnetosphere to smooth the PAD of high-energy protons. It has been proposed that pitch angle scattering could occur in near-Earth particles when the curvature radius is close to the gyroradius [*Sergeev et al.*, 1983, 1993; *Birmingham*, 1984; *Büchner and Zelenyi*, 1989; *Anderson et al.*, 1997; *Young et al.*, 2008]. *Sergeev et al.* [1983; 1993] suggested that it occurs when $R_C/R_L \leq 8$, where R_C and R_L are the curvature radius and the gyroradius, respectively. The critical energy for this process is given by

$$E_C = \frac{(qBR_C)^2}{2mK^2}, \tag{3}$$

where q is charge, K is the ratio between R_C and R_L, and m is mass. The simulated R_C is 0.37 Re at L = 5 in the equatorial plane at 0015 UT. Following *Sergeev et al.* [1983], we assumed critical K to be 8. The critical energy is then calculated to be 57 keV for a proton. The protons at 57 keV and above may have undergone a curvature-associated pitch angle scattering process that smoothes the PAD. It is likely that this estimation can explain the difference in the magnitude of the depression of high-energy fluxes (≥90 keV) between simulation and observation.

[28] The ring current effect is expected to be latitudinally confined near the equatorial plane where the magnetic field strength is weak and the plasma pressure is high. However, previous in situ observations in the outer radiation belt have shown that the ring current effect appears not only near the equatorial plane, but also at high latitudes where the magnetic field strength is strong (low β region) [*Li et al.*, 1997; *Nakamura et al.*, 1998]. On the basis of our simulation results, we predict the following processes probably acting on relativistic electrons in the outer radiation belt, which may explain the overall adiabatic depression of relativistic electrons at high latitudes. (1) Tens-of-keV ions move from the nightside plasma sheet to the inner region under a strong convection electric field, resulting in enhancement of the plasma pressure (and the ring current). (2) The enhanced plasma pressure depresses the local magnetic field near the equatorial plane. (3) The relativistic electrons undergo adiabatic deceleration near the equatorial plane (formation of a butterfly-like PAD near the equatorial plane). (4) A pitch angle scattering process, probably due to wave–particle interactions, makes the electron PAD more isotropic. (5) The electron flux near the loss cone decreases due to the pitch angle scattering process. Thus, the overall electron flux at high latitudes decreases.

[29] It should be emphasized that decreases in the relativistic electron fluxes can also be caused by loss of the electrons due to precipitation into the atmosphere and/or magnetopause encounter [e.g., *Shprits et al.*, 2006]. In the near future, ECRCM will be incorporated with the radiation belt electrons to test these possible processes and to investigate the overall coupling processes between the ring current ions and the radiation belt electrons.

6. Conclusion

[30] The major conclusions drawn in this paper are summarized as follows.

[31] 1. On the basis of data from the Polar satellite, the magnetic field is sometimes highly depressed by 50% or more near the equatorial plane at a radial distance less than 6 R_E. We call this the equatorially magnetic depression event (EMDE). In most cases, EMDEs are accompanied by a butterfly-like PAD of 100 keV proton flux.

[32] 2. Simulation of the ring current with a self-consistent magnetic field and electric fields predicts that when low-energy protons (<80 keV) are injected into the inner magnetosphere, the high-energy proton flux (>90 keV) adiabatically decreases (increases) at pitch angles near 90° (0° and 180°). The resultant PAD is butterfly-like. This tendency agrees well with the Polar satellite observations for the most intense EMDE.

[33] 3. The decrease in the simulated high-energy proton flux is much greater in magnitude and wider in pitch angle than in the observed ring current. Shortened curvature radius of a field line could cause pitch angle scattering which smoothes the PAD.

[34] 4. The enhancement of the low-energy protons (<80 keV) is expected to result in adiabatic reduction of the equatorially mirroring relativistic electrons and the resultant butterfly-like PAD. The adiabatic effect would act on not only the equatorially mirroring electrons but also on electrons. PADs of protons and electrons can be used as a quantitative measure of the ring current effect for the purpose of distinguishing nonadiabatic processes acting selectively on electrons from adiabatic one.

[35] **Acknowledgments.** IMF and solar wind data were provided by Norman Ness (ACE/MFI) and David J. McComas (ACE/SWEPAM) through NASA/GSFC/CDAWeb. The authors thank Nikolai A. Tsyganenko for providing the empirical magnetic field model; Daniel R. Weimer for providing the empirical convection electric field model; and Theodore A. Fritz, James L. Roeder, and Manuel Grande for providing the well-calibrated Polar/MICS data. This study was supported by the Program for Improvement of Research Environments for Young Researchers from the Special Coordination Funds for Promoting Science and Technology (SCF) commissioned by the Ministry of Education, Culture, Sports, Science and Technology (MEXT) of Japan.

References

Akasofu, S.-I., J. C. Cain, and S. Chapman (1961), The magnetic field of a model radiation belt, numerically computed, *J. Geophys. Res.*, *66*, 4013–4026, doi:10.1029/JZ066i012p04013.

Anderson, B., R. Decker, N. Paschalidis, and T. Sarris (1997), Onset of nonadiabatic particle motion in the near-Earth magnetotail, *J. Geophys. Res.*, *102*(A8), 17,553–17,569, doi:10.1029/97JA00798.

Baker, D. N., P. R. Higbie, E. W. Hones Jr., and R. D. Belian (1978), High-resolution energetic particle measurements at 6.6 RE: 3. Low-energy electron anisotropies and short-term substorm predictions, *J. Geophys. Res.*, *83*(A10), 4863–4868, doi:10.1029/JA083iA10p04863.

Baker, D. N., P. Stauning, E. W. Hones Jr., P. R. Higbie, and R. D. Belian (1981a), Near-equatorial, high-resolution measurements of electron precipitation at $L \simeq 6.6$, *J. Geophys. Res.*, *86*(A4), 2295–2313, doi:10.1029/JA086iA04p02295.

Baker, D. N., E. W. Hones Jr., P. R. Higbie, R. D. Belian, and P. Stauning (1981b), Global properties of the magnetosphere during a substorm growth phase: A case study, *J. Geophys. Res.*, *86*(A11), 8941–8956, doi:10.1029/JA086iA11p08941.

Berko, F., L. Cahill Jr., and T. Fritz (1975), Protons as the prime contributors to storm time ring current, *J. Geophys. Res.*, *80*(25), 3549–3552, doi:10.1029/JA080i025p03549.

Bilitza, D. (1997), International Reference Ionosphere-status, 1995/96, *Adv. Space Res.*, *20*, 1751–1754, doi:10.1016/S0273-1177(97)00584-X.

Birmingham, T. (1984), Pitch Angle Diffusion in the Jovian Magnetodisc, *J. Geophys. Res.*, *89*(A5), 2699–2707, doi:10.1029/JA089iA05p02699.

Blake, J. B., et al. (1995), CEPPAD: Comprehensive energetic particle and pitch angle distribution experiment on Polar, *Space Sci. Rev.*, *71*, 531–562, doi:10.1007/BF00751340.

Brandt, P. C., D. G. Mitchell, Y. Ebihara, B. R. Sandel, E. C. Roelof, J. L. Burch, and R. Demajistre (2002), Global IMAGE/HENA observations of the ring current: Examples of rapid response to IMF and ring current-plasmasphere interaction, *J. Geophys. Res.*, *107*(A11), 1359, doi:10.1029/2001JA000084.

Büchner, J., and L. M. Zelenyi (1989), Regular and chaotic charged particle motion in magnetotaillike field reversals: 1. Basic theory of trapped motion, *J. Geophys. Res.*, *94*(A9), 11,821–11,842, doi:10.1029/JA094iA09p11821.

Chen, M. W., S. Liu, M. Schulz, J. L. Roeder, and L. R. Lyons (2006), Magnetically self-consistent ring current simulations during the 19 October 1998 storm, *J. Geophys. Res.*, *111*, A11S15, doi:10.1029/2006JA011620.

Dessler, A. J., and R. Karplus (1961), Some effects of diamagnetic ring currents on Van Allen radiation, *J. Geophys. Res.*, *66*(8), 2289–2295, doi:10.1029/JZ066i008p02289.

Ebihara, Y., and M. Ejiri (2000), Simulation study on fundamental properties of the storm-time ring current, *J. Geophys. Res.*, *105*(A7), 15,843–15,859, doi:10.1029/1999JA900493.

Ejiri, M., R. A. Hoffman, and P. H. Smith (1980), Energetic particle penetrations into the inner magnetosphere, *J. Geophys. Res.*, *85*(A2), 653–663, doi:10.1029/JA085iA02p00653.

Fok, M.-C., R. A. Wolf, R. W. Spiro, and T. E. Moore (2001), Comprehensive computational model of Earth's ring current, *J. Geophys. Res.*, *106*(A5), 8417–8424, doi:10.1029/2000JA000235.

Fritz, T. A., M. Alothman, J. Bhattacharjya, D. L. Matthews, and J. Chen (2003), Butterfly pitch angle distributions observed by ISEE-1, *Planet. Space Sci.*, *51*(3), 205–219, doi:10.1016/S0032-0633(02)00202-7.

Fu, S. Y., B. Wilken, Q. G. Zong, and Z. Y. Pu (2001), Ion composition variations in the inner magnetosphere: Individual and collective storm effects in 1991, *J. Geophys. Res.*, *106*(A12), 29,683–29,704, doi:10.1029/2000JA900173.

Hardy, D. A., M. S. Gussenhoven, R. Raistrick, and W. J. McNeil (1987), Statistical and functional representations of the pattern of auroral energy flux, number flux, and conductivity, *J. Geophys. Res.*, *92*(A11), 12,275–12,294, doi:10.1029/JA092iA11p12275.

Hedin, A. E. (1991), Extension of the MSIS thermospheric model into the middle and lower atmosphere, *J. Geophys. Res.*, *96*(A2), 1159–1172, doi:10.1029/90JA02125.

Hoffman, R. A., and P. A. Bracken (1965), Magnetic effects of the quiet-time proton belt, *J. Geophys. Res.*, *70*(15), 3541–3556, doi:10.1029/JZ070i015p03541.

Hoffman, R. A., and P. A. Bracken (1967), Higher-order ring currents and particle energy storage in the magnetosphere, *J. Geophys. Res.*, *72*(23), 6039–6049, doi:10.1029/JZ072i023p06039.

Kim, H.-J., and A. A. Chan (1997), Fully adiabatic changes in storm time relativistic electron fluxes, *J. Geophys. Res.*, *102*(A10), 22,107–22,116, doi:10.1029/97JA01814.

Krimigis, S., G. Gloeckler, R. McEntire, T. Potemra, F. Scarf, and E. Shelley (1985), Magnetic Storm of September 4, 1984: A Synthesis of Ring Current Spectra and Energy Densities Measured with AMPTE/CCE, *Geophys. Res. Lett.*, *12*(5), 329–332, doi:10.1029/GL012i005p00329.

Le, G., C. T. Russell, and K. Takahashi (2004), Morphology of the ring current derived from in-situ magnetic field measurements, *Ann. Geophys.*, *22*, 1267–1295.

Lemon, C., R. A. Wolf, T. W. Hill, S. Sazykin, R. W. Spiro, F. R. Toffoletto, J. Birn, and M. Hesse (2004), Magnetic storm ring current injection modeled with the Rice Convection Model and a self-consistent magnetic field, *Geophys. Res. Lett.*, *31*, L21801, doi:10.1029/2004GL020914.

Li, X., D. N. Baker, M. Temerin, T. E. Cayton, E. G. D. Reeves, R. A. Christensen, J. B. Blake, M. D. Looper, R. Nakamura, and S. G. Kanekal (1997), Multisatellite observations of the outer zone electron variation during the November 3–4, 1993, magnetic storm, *J. Geophys. Res.*, *102*(A7), 14,123–14,140, doi:10.1029/97JA01101.

Li, X., D. Baker, M. Temerin, W. Peterson, and J. Fennell (2000), Multiple Discrete-Energy Ion Features in the Inner Magnetosphere: Observations

and Simulations, *Geophys. Res. Lett.*, *27*(10), 1447–1450, doi:10.1029/1999GL010745.

Lyons, L. R. (1977), Adiabatic evolution of trapped particle pitch angle distributions during a storm main phase, *J. Geophys. Res.*, *82*(16), 2428–2432, doi:10.1029/JA082i016p02428.

Lyons, L., and D. Williams (1976), Storm-associated variations of equatorially mirroring ring current protons, 1–800 keV, at Constant First Adiabatic Invariant, *J. Geophys. Res.*, *81*(1), 216–220, doi:10.1029/JA081i001p00216.

McIlwain, C. E. (1966), Ring current effects on trapped particles, *J. Geophys. Res.*, *71*(15), 3623–3628.

Morioka, A., H. Misawa, Y. Miyoshi, H. Oya, M. Iizima, and T. Nagai (2001), Pitch angle distribution of relativistic electrons in the inner radiation belt and its relation to equatorial plasma wave turbulence phenomena, *Geophys. Res. Lett.*, *28*(5), 931–934, doi:10.1029/2000GL011886.

Nakamura, R., K. Kamei, Y. Kamide, D. Baker, J. Blake, and M. Looper (1998), SAMPEX observations of storm-associated electron flux variations in the outer radiation belt, *J. Geophys. Res.*, *103*(A11), 26,261–26,269, doi:10.1029/97JA02873.

Orsini, S., I. A. Daglis, M. Candidi, K. C. Hsieh, S. Livi, and B. Wilken (1994), Model calculation of energetic neutral atoms precipitation at low altitudes, *J. Geophys. Res.*, *99*(A7), 13,489–13,498, doi:10.1029/93JA03270.

Pfitzer, K., T. W. Lezniak, and J. R. Winckler (1969), Experimental verification of drift shell splitting in the distorted magnetosphere, *J. Geophys. Res.*, *74*(19), 4687–4693, doi:10.1029/JA074i019p04687.

Roederer, J. G. (1967), On the adiabatic motion of energetic particles in a model magnetosphere, *J. Geophys. Res.*, *72*(3), 981–992, doi:10.1029/JZ072i003p00981.

Roeder, J. L., M. W. Chen, J. F. Fennell, and R. Friedel (2005), Empirical models of the low-energy plasma in the inner magnetosphere, *Space Weather*, *3*, S12B06, doi:10.1029/2005SW000161.

Russell, C. T., R. C. Snare, J. D. Means, D. Pierce, D. Dearborn, M. Larson, G. Barr, and G. Le (1995), The GGS/Polar magnetic fields investigation, it, *Space Sci. Rev.*, *71*, 563–582, doi:10.1007/BF00751341.

Selesnick, R. S., and J. B. Blake (2002), Relativistic electron drift shell splitting, *J. Geophys. Res.*, *107*(A9), 1265, doi:10.1029/2001JA009179.

Sergeev, V. A., E. M. Sazhina, N. A. Tsyganenko, J. Å. Lundblad, and F. Søraas (1983), Pitch-angle scattering of energetic protons in the magnetotail current sheet as the dominant source of their isotropic precipitation into the nightside ionosphere, *Planet. Space Sci.*, *31*, 1147–1155, doi:10.1016/0032-0633(83)90103-4.

Sergeev, V. A., M. Malkov, and K. Mursula (1993), Testing the isotropic boundary algorithm method to evaluate the magnetic field configuration in the tail, *J. Geophys. Res.*, *98*(A5), 7609–7620, doi:10.1029/92JA02587.

Sheldon, R. B., and D. C. Hamilton (1993), Ion transport and loss in the Earth's quiet ring current: 1. Data and standard model, *J. Geophys. Res.*, *98*(A8), 13,491–13,508, doi:10.1029/92JA02869.

Shprits, Y. Y., R. M. Thorne, R. Friedel, G. D. Reeves, J. Fennell, D. N. Baker, and S. G. Kanekal (2006), Outward radial diffusion driven by losses at magnetopause, *J. Geophys. Res.*, *111*, A11214, doi:10.1029/2006JA011657.

Sibeck, D. G., R. W. McEntire, A. T. Y. Lui, R. E. Lopez, and S. M. Krimigis (1987), Magnetic field drift shell splitting: Cause of unusual dayside particle pitch angle distributions during storms and substorms, *J. Geophys. Res.*, *92*, 13,485–13,497.

Smith, P., and R. Hoffman (1974), Direct observations in the dusk hours of the characteristics of the storm time ring current particles during the beginning of magnetic storms, *J. Geophys. Res.*, *79*(7), 966–971, doi:10.1029/JA079i007p00966.

Söraas, F., and L. R. Davis (1968), Temporal variations of the 100 keV to 1700 keV trapped protons observed on satellite Explorer 26 during first half of 1965, *Rep. X-612–68–328*, NASA Goddard Space Flight Cent., Greenbelt, Md.

Stone, E. C. (1963), The physical significance of and application of L, B_0 and R_0 to geomagnetically trapped particles, *J. Geophys. Res.*, *68*, 4157–4166.

Tsyganenko, N. A. (1995), Modeling the Earth's magnetospheric magnetic field confined within a realistic magnetopause, *J. Geophys. Res.*, *100*(A4), 5599, doi:10.1029/94JA03193.

Tsyganenko, N. A., and D. P. Stern (1996), A new-generation global magnetosphere field model, based on spacecraft magnetometer data, *ISTP Newsl.*, *6*(1), 21.

Weimer, D. R. (2001), An improved model of ionospheric electric potentials including substorm perturbations and application to the Geospace Environment Modeling November 24, 1996, event, *J. Geophys. Res.*, *106*(A1), 407–416, doi:10.1029/2000JA000604.

West, H. I., Jr., R. M. Buck, and J. R. Walton (1973), Electron pitch angle distributions of energetic electrons throughout the magnetosphere as observed on OGO 5, *J. Geophys. Res.*, *78*(7), 1064–1081, doi:10.1029/JA078i007p01064.

Wilken, B., et al. (1992), Magnetospheric ion composition spectrometer onboard the CRRES spacecraft, *J. Spacecr. Rockets*, *29*(4), 585–591, doi:10.2514/3.25503.

Williams, D. J. (1981a), Phase space variations of near equatorially mirroring ring current ions, *J. Geophys. Res.*, *86*(A1), 189–194, doi:10.1029/JA086iA01p00189.

Williams, D. J. (1981b), Ring current composition and sources: An update, *Planet. Space Sci.*, *29*, 1195–1203, doi:10.1016/0032-0633(81)90124-0.

Williams, D., J. Arens, and L. Lanzerotti (1968), Observations of trapped electrons at low and high altitudes, *J. Geophys. Res.*, *73*(17), 5673–5696, doi:10.1029/JA073i017p05673.

Young, S. L., R. E. Denton, B. J. Anderson, and M. K. Hudson (2008), Magnetic field line curvature induced pitch angle diffusion in the inner magnetosphere, *J. Geophys. Res.*, *113*, A03210, doi:10.1029/2006JA012133.

Zaharia, S., V. K. Jordanova, M. F. Thomsen, and G. D. Reeves (2006), Self-consistent modeling of magnetic fields and plasmas in the inner magnetosphere: Application to a geomagnetic storm, *J. Geophys. Res.*, *111*, A11S14, doi:10.1029/2006JA011619.

Y. Ebihara, Institute for Advanced Research, Nagoya University, Furocho, Chikusa-ku, Nagoya, 464-8601, Japan. (ebihara@stelab.nagoya-u.ac.jp)

J. B. Blake and J. F. Fennell, Space Sciences Department, Aerospace Corporation, P. O. Box 92957, Los Angeles, CA 90009-2957, USA.

M.-C. Fok, NASA Goddard Space Flight Center, Code 673, Greenbelt, MD 20771, USA.